Smart Structures and Systems, Vol. 3, No. 1 (2007) 23-49
DOI: http://dx.doi.org/10.12989/sss.2007.3.1.023

Wavelet analysis and enhanced damage indicators

N. Lakshmanan†

Structural Engineering Research Centre, CSIR Campus, Taramani, Chennai, 600113, India

B. K. Raghuprasad‡

Department of Civil Engineering, Indian Institute of Science, Bangalore, 560012, India

K. Muthumani‡†, N. Gopalakrishnan‡† and D. Basu‡†

Structural Engineering Research Centre, CSIR Campus, Taramani, Chennai, 600113, India

(Received May 24, 2005, Accepted June 7, 2006)

Abstract. Wavelet transforms are the emerging signal-processing tools for damage identification and time-frequency localization. A small perturbation in a static or dynamic displacement profile could be captured using multi-resolution technique of wavelet analysis. The paper presents the wavelet analysis of damaged linear structural elements using DB4 or BIOR6.8 family of wavelets. Starting with a localized reduction of EI at the mid-span of a simply supported beam, damage modeling is done for a typical steel and reinforced concrete beam element. Rotation and curvature mode shapes are found to be the improved indicators of damage and when these are coupled with wavelet analysis, a clear picture of damage singularity emerges. In the steel beam, the damage is modeled as a rotational spring and for an RC section, moment curvature relationship is used to compute the effective EI. Wavelet analysis is performed for these damage models for displacement, rotation and curvature mode shapes as well as static deformation profiles. It is shown that all the damage indicators like displacement, slope and curvature are magnified under higher modes. A localization scheme with arbitrary location of curvature nodes within a pseudo span is developed for steady state dynamic loads, such that curvature response and damages are maximized and the scheme is numerically tested and proved.

Keywords: wavelet transforms; damage identification; modal parameters; enhanced damage indicators.

1. Introduction

Research in the area of damage detection and identification through changes in the fundamental frequencies and modal parameters of a structure saw a quantum jump during late eighties and early nineties (Lakshmanan, *et al.* 1991, Rajagopalan, *et al.* 1996, 1999, Hassiotis, *et al.* 1993, Hassiotis 2000). This is in spite of the fact that natural frequency is a less sensitive parameter to structural damage. If it is assumed that $(EI)_{eff}$ undergoes a global change 'α', then change in the natural frequency could be

†Scientist, Corresponding Author, E-mail: ng@sercm.org
‡Professor
‡†Scientist

approximated as 0.5α. Also, if a quadratic relationship is assumed between the strength and modulus, as typical of concrete, with E proportional to $\sqrt{f_{ck}}$, natural frequency is proportional to $\sqrt{f_{ck}^{0.25}}$. This implies that if a 20% drop occurs in the strength of a system, its natural frequency drops by 5%. On the contrary, increase in static deflection is directly proportional to the decrease in $(EI)_{eff}$. Nevertheless, damage identification is still pursued through dynamic measurement techniques by engineers and scientists, due to the following reasons:

(a) Progress made in digital electronics has propelled an enormous spurt in the dynamic measurement techniques involving smart, laser based and MEMS sensors, data acquisition and wireless communications. The technology of transducers and the connected integrated circuits and amplifiers, have seen enormous miniaturization, capacity increase, coupled with sharp fall in their price. The sensitivity of the instruments increased in orders of magnitude and even a small force is sufficient to excite a structure to its natural frequencies.

(b) Whereas an elaborate amount of instrumentation and mounting system is required to evaluate a structure under in-situ conditions with static loading, well reduced paraphernalia is sufficient for the dynamic response measurements with ambient excitations.

(c) Techniques like fast Fourier transforms have been embedded into the chips to form firmware and these analyzers have also been made portable for easy field use. The idea of condition monitoring has crept into civil engineering with periodic collection and Fourier synthesis of vibration signatures being made mandatory for certain bridges.

(d) More than natural frequencies and displacement mode shapes, rotation and curvature mode shapes are better indicators of damage and these coupled with appropriate signal enhancement techniques could be used as ideal damage indicators (Pandey, *et al.* 1991, Abdel Wahab, *et al.* 1999, Ratcliffe 2000, Abdo, *et al.* 2002, Owolabi, *et al.* 2003).

(e) Measurement of modal parameters could be used to work back the system characteristics like stiffness, flexibility and mass distribution (Sheinman 1996).

(f) Development of new signal processing techniques like wavelet transforms have entered in a large way in structural engineering as a tool to magnify the localized damages in mode shapes and for other applications. (Liew, *et al.* 1998, Gurley, *et al.* 1999, Hou, *et al.* 2000, Melhem, *et al.* 2003, Hera, *et al.* 2004, Kim, *et al.* 2004).

(g) Wave propagation techniques with sonic, ultra-sonic and electro-magnetic waves are the other promising damage detection tools.

2. Crack modelling

Two models are available for modeling a defect or a crack in a linear structural member like a beam or column.

2.1. Model-1

In the case of a ductile material like steel, a crack may already exist and can start growing under cyclic loads. The zone over which the crack exists is in fact a length tending towards zero and hence a zone of reduced flexural rigidity could not be conveniently adopted. However a sudden change in the flexural rigidity occurs and the model adopted in the present work is through idealizing a transversely cracked section with an equivalent rotational spring of particular spring stiffness. The rotational spring stiffness is a function of the ratio of the length of a crack to the depth of section. Linear elastic fracture mechanics principles could be used to establish the spring stiffness of a cracked section.

2.2. Model-2

In the second model, representing a reinforced concrete element, each section has a reduced $(EI)_{eff}$, depending upon the moment, axial and shear force carried by the member. Typically the moment curvature (M-ϕ) relationship of a reinforced concrete structural member, dominated by flexure could be estimated, using a fibre theory. Neutral axis depth is sequentially progressed with varying concrete strains at extreme fiber, such that force equilibrium is achieved. The moment-curvature pair, giving rise to such equilibrium state could then be estimated. This can also be calculated using reasonably valid approximated expressions, using a tri-linear (M-ϕ) relationship, denoting the transition between cracking, yielding and ultimate moment stages. The effect of axial force could also be accounted in estimating such relationships. The slope of the moment curvature curve could then be used to estimate $(EI)_{eff}$ at a particular section depending on the moment carried by that section. A quasi-brittle material like concrete, combined with reinforcing steel and having a large number of closely spaced cracks, under conditions of high bond stress between steel and concrete could be conveniently represented by an $(EI)_{eff}$ model, both for calculating deflections and also for computing the natural frequencies of a flexure-dominated beam.

3. Mathematical foundations of wavelet transforms

Wavelets are localized and compact signals, oscillating for a few cycles about a zero mean. A basic wavelet function can have time or space as its independent variable. For damage identification purposes, space (length) is used as the independent variable. In time-frequency analysis, time is used as the independent variable. The basic wavelet function, called as 'mother wavelet', $\psi(x)$, can be stretched or compressed by 'a' and translated in space by 'b', to generate a set of basis functions.

$$\psi_{a,b}(x) = \frac{1}{\sqrt{a}}\psi\left(\frac{x-b}{a}\right) \tag{1}$$

Coefficients of continuous wavelet transform (CWT) of any function are obtained by integrating the dilated and translated mother wavelet with the given function for the entire space.

$$C(a,b) = \frac{1}{\sqrt{a}}\int_{-\infty}^{\infty} f(x)\cdot\psi\left(\frac{x-b}{a}\right)dx \tag{2}$$

The wavelet transform results in coefficients, that indicates how well a wavelet function of a particular dilation and translation correlates with the given function. Sharp and sudden variations in $f(x)$ result in large wavelet coefficients and hence the localized singularity in space or time could be captured. Unlike a Fourier transform, a one-dimensional function results in two dimensional wavelet coefficients. In a Fourier analysis, any function defined within a range of span or time can be written as the sum of sinusoidal functions of different periods (integral multiples of the given period) and whose amplitudes depend on the correlation of the original waveform with the particular sinusoid. A wavelet transform is similar to the Fourier transform, but the original function is the combination of many dilated and translated wavelets in time or space. A waveform reconstruction is possible using the mother wavelet and this is mathematically stated as,

$$\frac{1}{K_{\psi}} \int_{-\infty}^{\infty} \int_{-\infty}^{\infty} C(a, b) \cdot \psi_{a, b}(x) \cdot db \cdot \frac{da}{a^2} \tag{3}$$

It can be proved that CWT is redundant and it is not necessary to use the full domain of $C(a, b)$ to reconstruct the original waveform. Instead of a continuum of dilations and translations, discrete values can be used. Dilation and translation parameters are defined as $a = 2^j$ and $b = k2^j$, where j and k are varying integers. Discrete wavelet transform (DWT) could be defined as,

$$C_{j, k} = 2^{-j/2} \int_{-\infty}^{\infty} f(x) \cdot \psi(2^{-j} \cdot x - k) dx \tag{4}$$

Similarly, signal reconstruction of DWT is defined by the following equation

$$f(x) = \sum_{j = -\infty}^{\infty} \cdot \sum_{k = -\infty}^{\infty} C_{j, k} \cdot 2^{-j/2} \cdot \psi(2^{-j} \cdot x - k) \tag{5}$$

Suppose that wavelet transform is available only for small scales, $a < a_0$, then another function $\phi(x)$, called scaling function has to be introduced. A scaling function may not exist for every wavelet and the existence of the scaling function is the pre-requisite for computation of fast wavelet transforms (FWT). It is possible to re-construct the original function as the sum of its approximations at level J plus all its details up to the same level.

$$f(x) = A_j(x) + \sum_{j \le J} D_j(x) \tag{6}$$

Eq. (6) is actually part of a larger equation, derived for multi-resolution analysis, stated as,

$$f(x) = \sum_{j = -\infty}^{J} \left(\sum_{k = -\infty}^{\infty} cD_j(k) \cdot \psi_{j, k}(x) \right) + \sum_{k = -\infty}^{\infty} cA_j(k) \cdot \phi_{j, k}(x) \tag{7}$$

In the above equation, the first part is the detail function and the second part is the approximation function. In other words,

$$D_j(k) = \sum_{k = -\infty}^{\infty} cD_j(k) \cdot \psi_{j, k}(x) \tag{8}$$

$$A_j(k) = \sum_{k = -\infty}^{\infty} cA_j(k) \cdot \phi_{j, k}(x) \tag{9}$$

The above functions reiterate that the original function at any level J, can be decomposed into an approximation function, (typically of low frequency) and a number of detailed functions up to level *J*. (typically of higher frequencies). Perturbations and singularities, in the form of sudden variations are captured in the detail (*D*) functions. Un-perturbed original waveform is retained through approximate (*A*) functions.

4. Mode shapes of a simply supported beam with a central defect

The simply supported beam is of 5m span and has a defect at the center (Fig. 1). The defect is idealized as a reduced $(\mathrm{EI})_{eff}$ having a 50% reduction as compared to the rest of the beam. The reduced EI is spread over a length of 0.25 m (5% of the total length). The beam is idealized as a two dimensional beam with 200 elements for the span length. The length of a sub-element is thus 0.025 m. A sub space iteration technique is used to extract the first 15 modes of the beam with a lumped mass formulation. The rotation and curvature variation of the mode shapes are also obtained. Fig. 2 shows the curvature mode shapes for the fundamental as well as higher modes. Since the reduction in EI is half, curvature shoots up by a factor of 2. Higher modes exhibits higher curvature as the second derivative of the mode shape varies faster compared to the displacement. Curvature is computed using the following central difference equation,

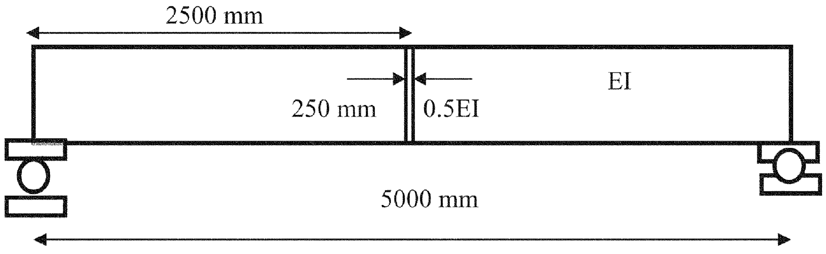

Fig. 1 Example of a simply supported beam used in the study

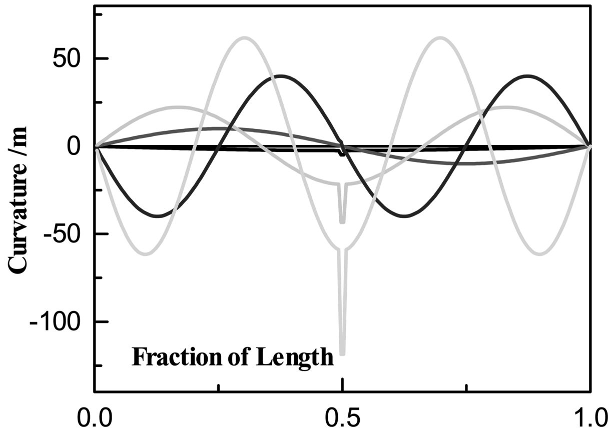

Fig. 2 Curvature variation of defective beam for fundamental and higher modes

$$\frac{M}{\mathrm{EI}} = -\frac{d^2y}{dx^2} = \frac{y_{n+1} - 2y_n + y_{n-1}}{\Delta h^2} = \frac{\theta_{n+1} - \theta_n}{\Delta h} \tag{10}$$

The idea of increased curvature for higher modes is understood by the following logic, using the example of the mode shape of simply supported beam.

$$\phi_N = A\sin\left(\frac{\pi N x}{l}\right)$$

$$\phi''_N = -A\left(\frac{\pi N}{l}\right)^2 \sin\left(\frac{\pi N x}{l}\right)$$

$$\phi''_N = -A\left(\frac{\pi}{l/N}\right)^2 \sin\left(\frac{\pi N x}{l}\right) \tag{11}$$

For example, the fifth mode of a beam shall have a curvature, equal to 25 times more than the first mode. The other way of visualizing this is that if the defect is spread over a length of γl for the original beam, the same beam shall have a pseudo span reduced by N times, when vibrating in 'N-th' mode. In

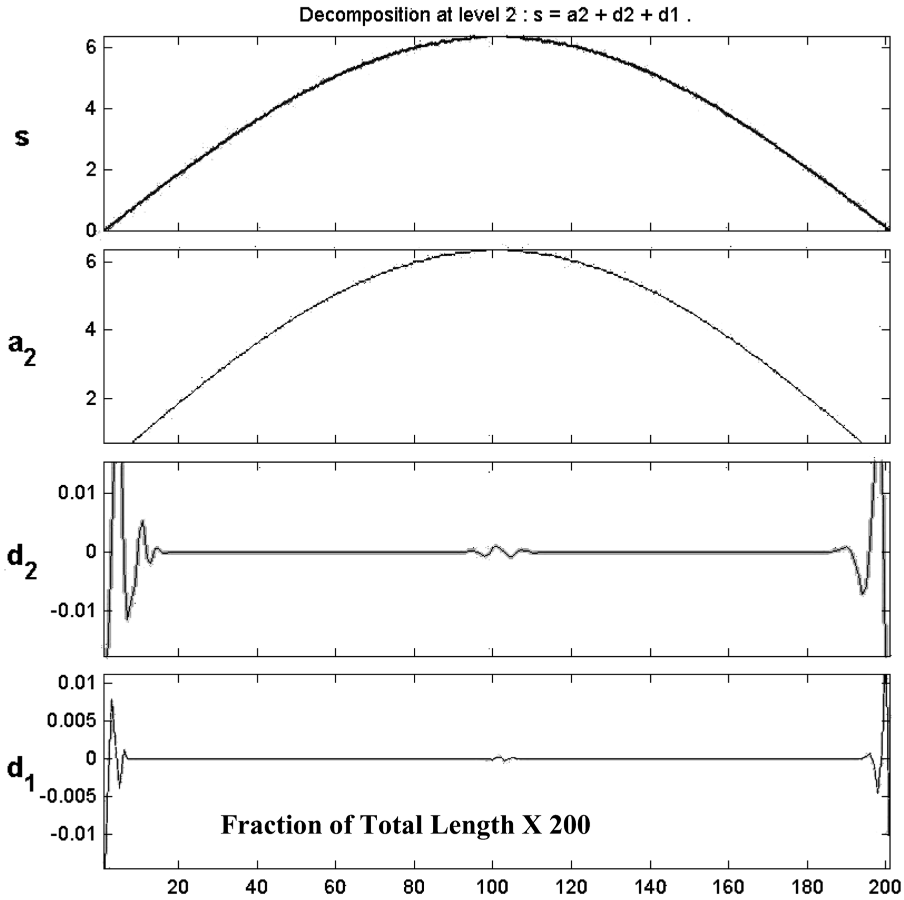

Fig. 3 Wavelet multi resolution analysis of the displacement mode of the defective beam for Mode-I

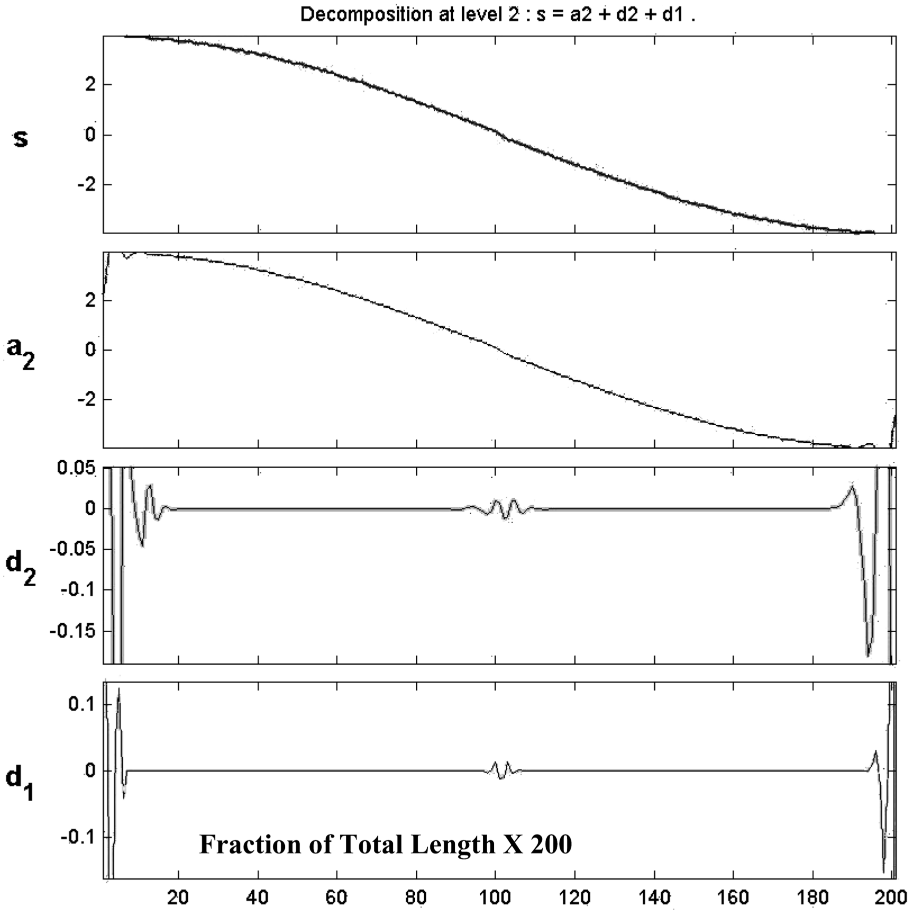

Fig. 4 Wavelet multi resolution analysis of the rotation mode of defective beam for Mode-I

other words, there is an apparent increase in the ratio of the defective length to the pseudo-span length by N times when measurements are carried at N-th mode. Further curvature jumps up as a square of this ratio. Wavelet multi resolution analysis of the displacement and rotation mode shapes is also performed and the results are shown in Figs. 3 to 8. Daubechies (DB4) and bi-orthogonal (BIOR 6.8) family of wavelets, available in MATLAB wavelet tool-box suite are used for the computation of the approximate and detail functions. Two level multi-resolution analysis is found to be sufficient to capture the disturbances in the deformation profile.

The ratio of detail D2 magnitudes as compared to the original signal values for displacement mode shapes are 0.02, 0.1 and 0.4% respectively for the first, third and fifth modes. Similarly, the ratio of detail D2 magnitudes as compared to the original signal values for rotation mode shapes are 0.5, 1.0 and 2.0% respectively for the first, third and fifth modes. These perturbations in the detail coefficients are similar to the high frequency content of a time frequency signal and in actual measurements a minimum threshold signal is always required such that it is above the electrical noise of the measuring instrument. In this context, the displacement perturbations, particularly for lower modes may not cross the noise threshold values of the measuring instrumentation. The even modes do not show any

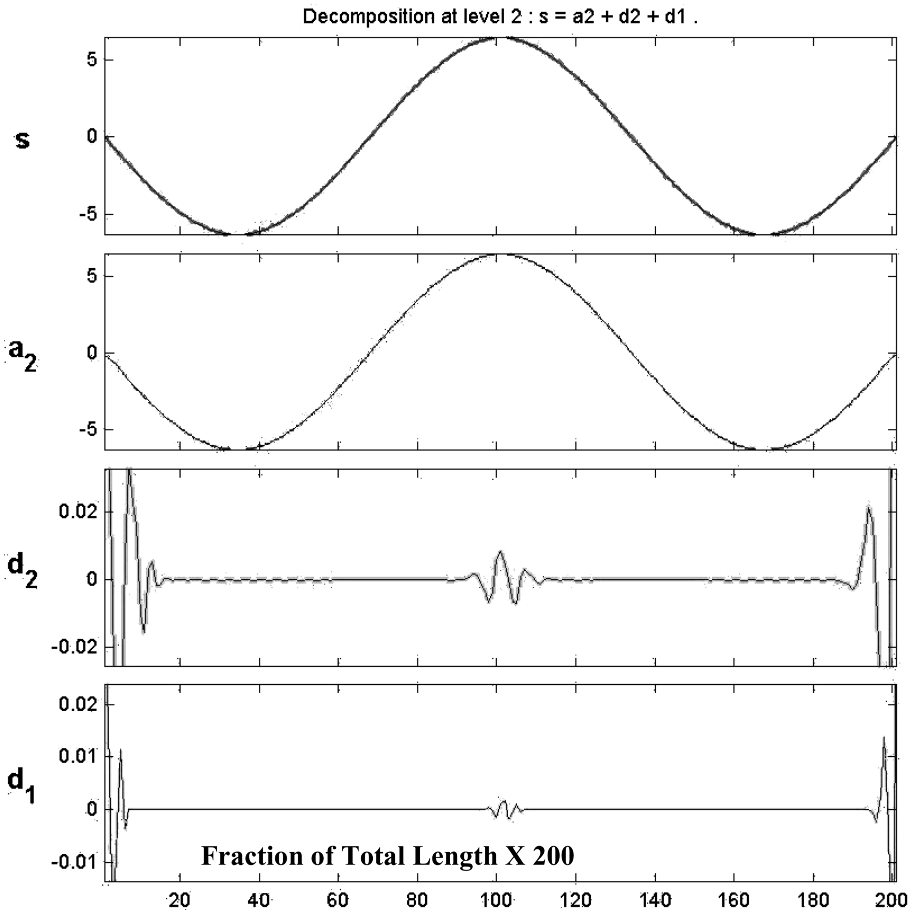

Fig. 5 Wavelet multi resolution analysis of the displacement mode of defective beam for Mode-III

perturbations both in displacement as well as rotation mode shapes as the defect is situated at the displacement node position of these modes.

5. Static response of the beam with an off-centric defect

Static deflected shape of the same beam is computed for a concentrated load applied at the center. A concentrated load causes a linear bending moment diagram and there is a third derivative discontinuity (in shear force variation) of the displacement profile. Hence the defect is shifted to a position of 0.2l from the support. Here too, the defect is idealized as a reduced $(EI)_{eff}$ having a 50% reduction as compared to the rest of the beam. The reduced EI is spread over a length of 0.25 m (5% of the total length), with its center located at 0.2l from the support. The beam is idealized as a two dimensional beam with 200 elements for the span length and here too, length of a sub-element is kept as 0.025 m. The curvature variation is plotted in Fig. 9 and it exactly follows the bending moment variation of the simply supported beam. The defect shows up as doubled up curvature value at the 0.2l position.

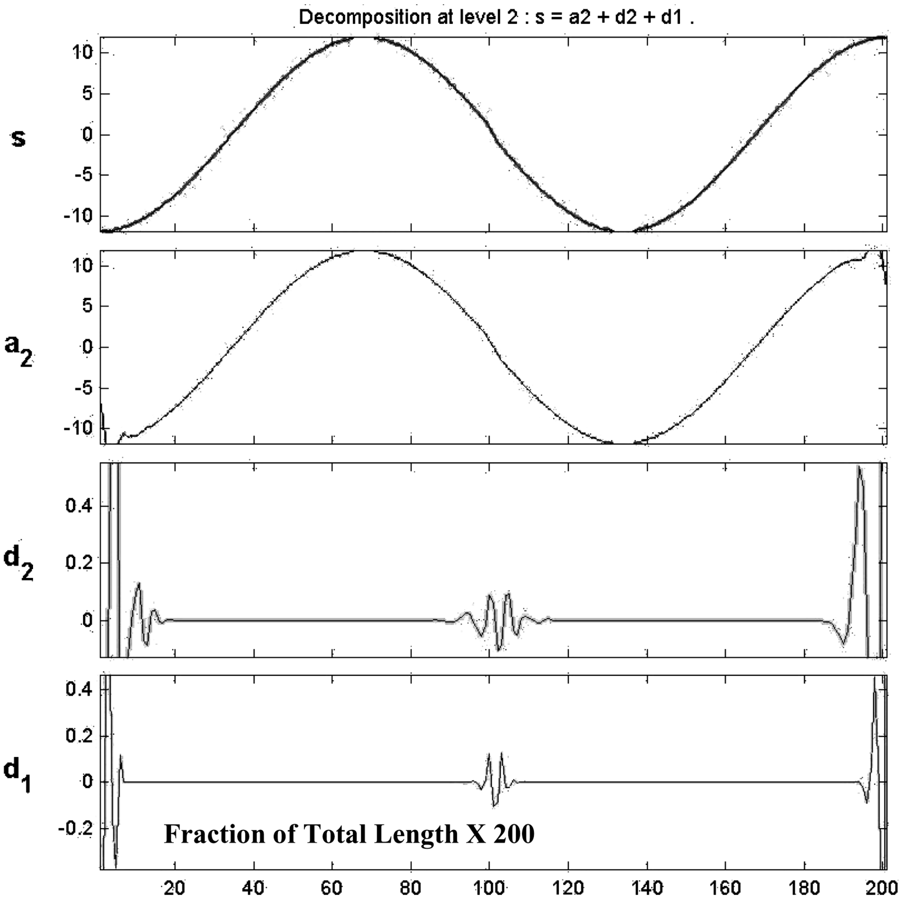

Fig. 6 Wavelet multi resolution analysis of the rotation mode of defective beam for Mode-III

Wavelet analysis is performed for both the displacement as well as rotation mode shapes. The detail coefficients hardly show up in displacement profile whereas the rotation profile shows up small disturbances (Fig. 10). A disturbance occurs below the concentrated load also due to the third derivative discontinuity of the displacement. This particular problem is unlikely to occur for dynamic loads as the loading is due to distributed effect of mass. The arguments of the previous case hold true in this case also and the displacement perturbations, may sometimes be buried within the random noise field of the measuring instrumentation.

6. Dynamic response of a steel beam with a central crack (Model-1)

The model which uses a reduced EI for modeling a local damage is sometimes good enough, but a real cracked section, with the length of the crack tending towards zero, is similar to a Dirac's delta function used in representing a singularity, with the integrated damage value being finite. As length of the crack is small, the curvature jump is infinite, but the rotation sees a definite discontinuity across the

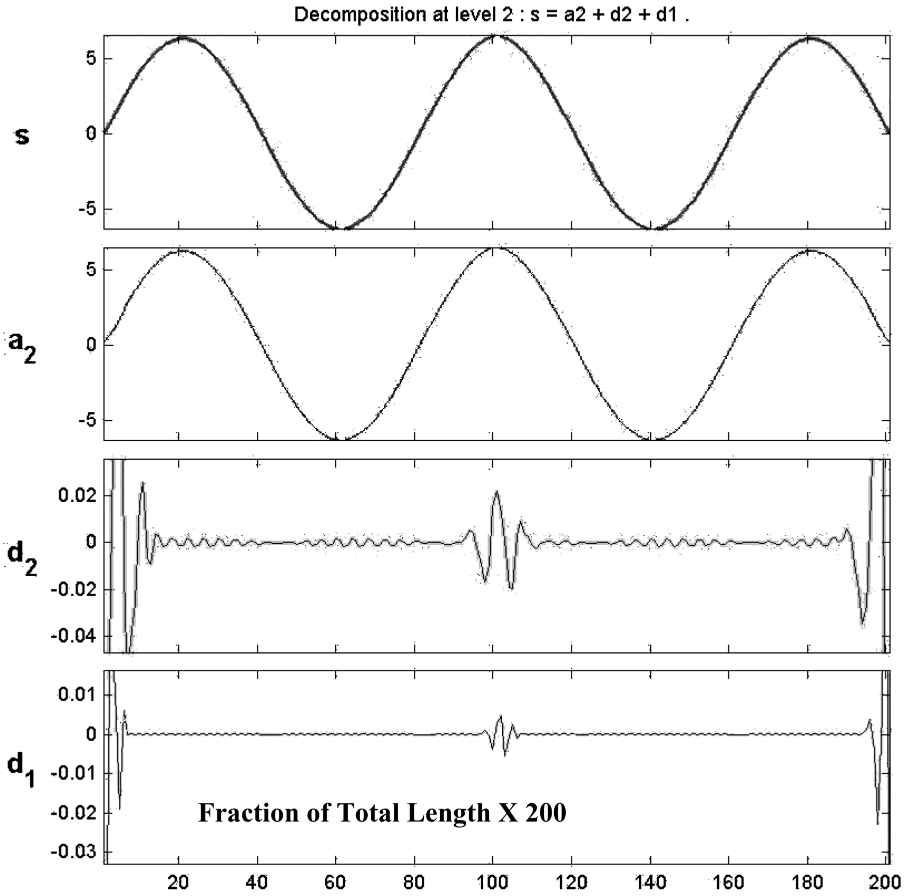

Fig. 7 Wavelet multi resolution analysis of the displacement mode of defective beam for Mode-V

crack. The transversely located physical crack existing in a steel structure for part of the depth and potentially growing in Mode-I fashion due to cyclic effects is modeled as a rotational spring. It is possible to find out the rotational spring stiffness of a cracked section, if the ratio of the depth of the crack with reference to the depth of the section is known, using principles of liner elastic fracture mechanics.

Fig. 11 shows the modeling of such a crack using rotational spring element. If the spring is very stiff, rotation difference across the plane of the crack is preserved and vice versa, there shall exist a discontinuity of slopes. The boundary conditions for these crack modeling include

(a) Moment, shear force and displacement continuity across the crack section

(b) Product of the rotational spring stiffness and the difference in the rotations on the two sides of the crack is equal to the external bending moment

The program is modified to account for rotation springs and the spring stiffness corresponds to a partial value of depth of the crack.

Wavelet analysis results of the rotation mode shapes are shown in Fig. 12 to Fig. 14, for the first, third and fifth modes. Detail coefficient (D1) and the related function values are more, when compared to (D2), unlike the previous cases, due to the fact that the crack is sharp and represents high frequency

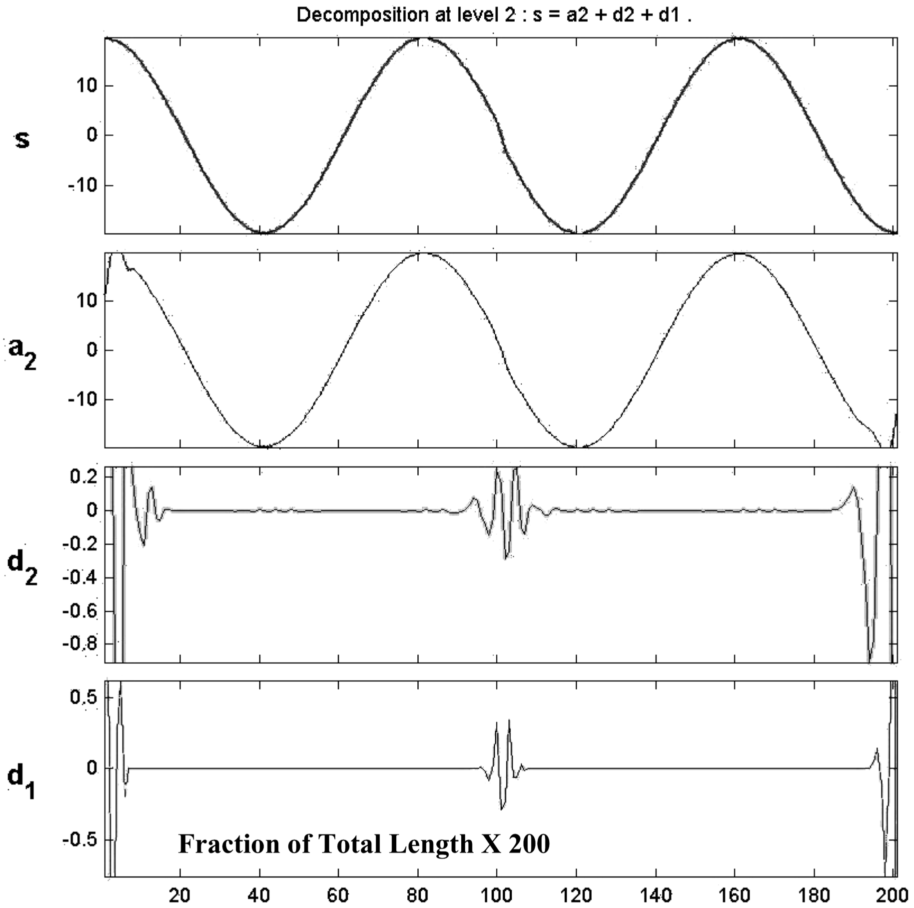

Fig. 8 Wavelet multi resolution analysis of the rotation mode of defective beam for Mode-V

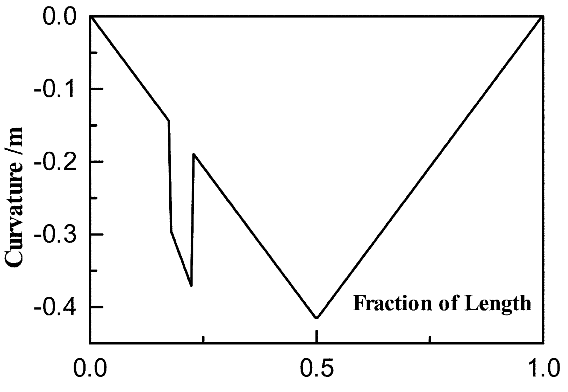

Fig. 9 Curvature variation for the static load case

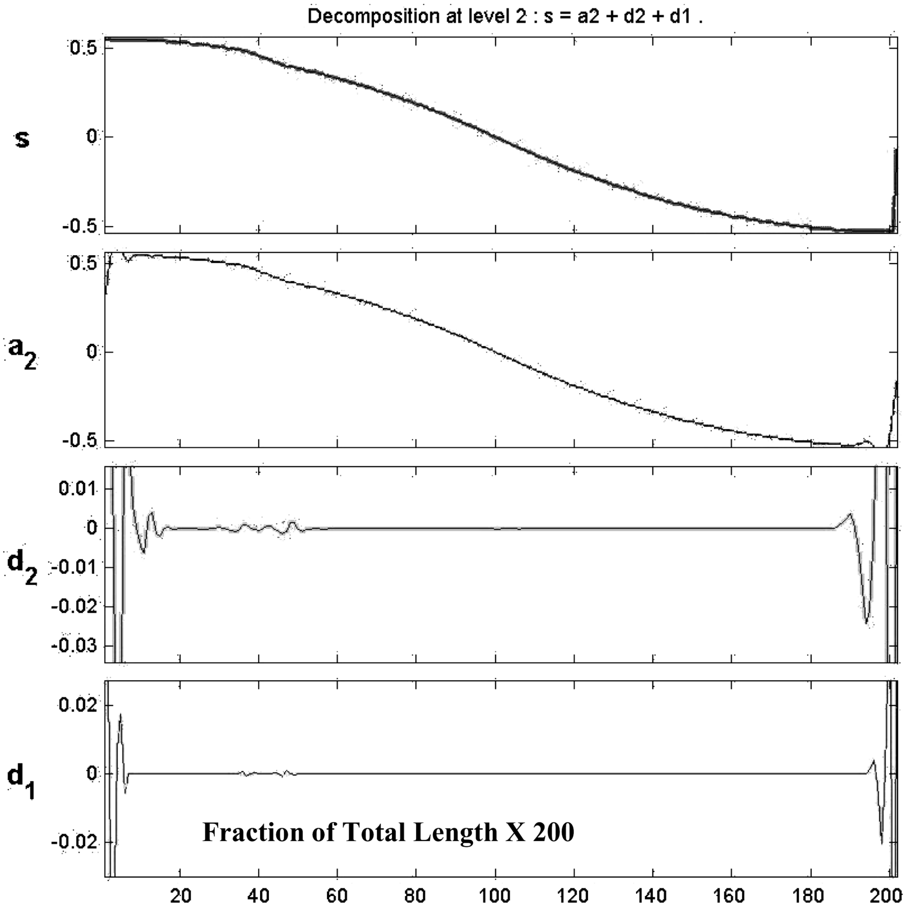

Fig. 10 Wavelet multi resolution analysis of the rotation of static deflected shape

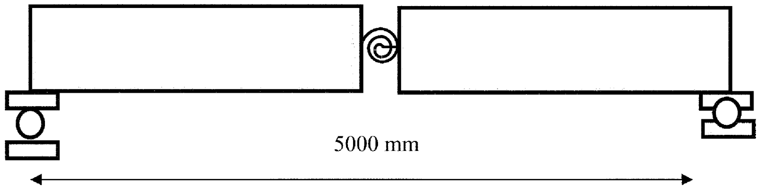

Fig. 11 Model to represent a transverse crack in a steel beam

variation, whereas in the previous values the crack existed for larger lengths (5%). The ratio of detail function magnitudes as compared to the original signal values for rotation mode shapes are 1.25, 5.0 and 10.0% respectively for the first, third and fifth modes.

It is necessary to examine the reason for the enhanced perturbation values exhibited at higher modes. Previously it is argued that the longitudinal dimension of the crack is considerable when compared to the pseudo span length of the beam at higher modes, where pseudo span length is defined as part of the length of the beam, between two consecutive curvature nodes. The results show the same trend in this model too, even though the length of the crack is nearly zero. The spring stiffness of the rotation spring,

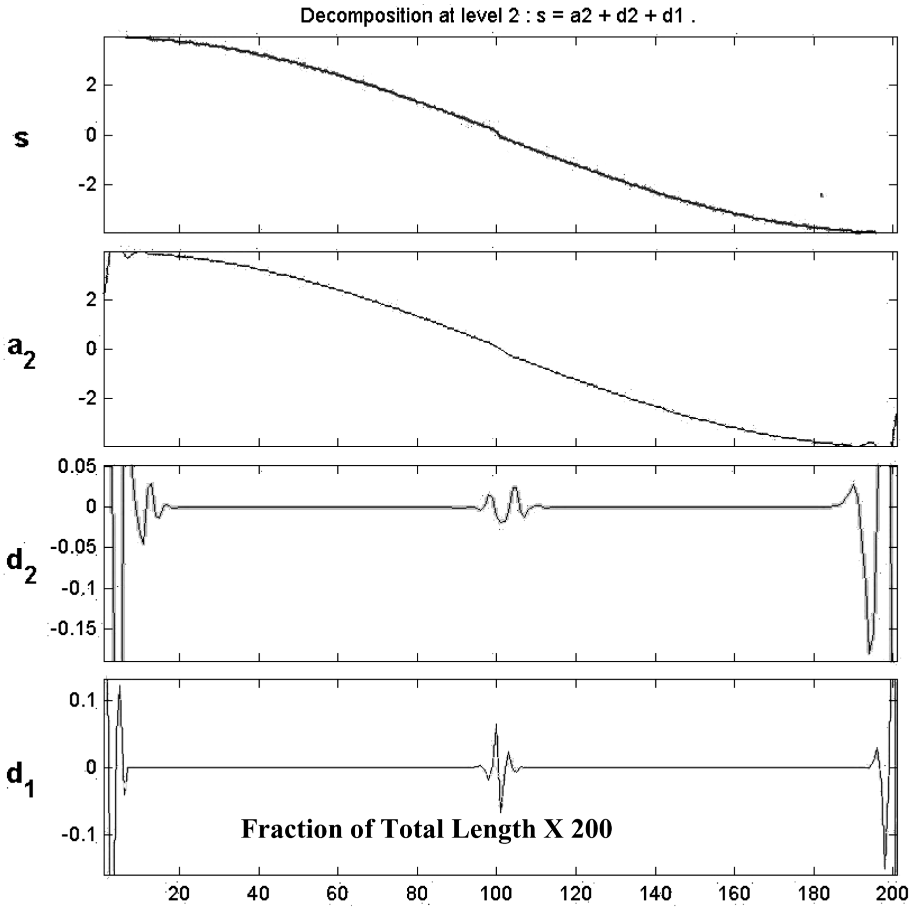

Fig. 12 Wavelet multi resolution analysis of the rotation mode shape for steel beam – Mode-I

representing a transversely cracked plane is high compared to the original length of the beam. In higher modes, the length of beam between the crack and the adjacent point of zero curvature falls by '*N*' times and thus the ratio of the crack-spring with reference to the rotation spring stiffness of the pseudo-beam, falls, thus showing more perturbation coefficients at higher modes.

7. Dynamic response of a reinforced concrete beam at three stages of loadings (Model-2)

The damage occurs in a reinforced concrete beam due to excessive loading, steel corrosion and ageing. The damage shows up in the form of excessive crack widths, deflection and lowered natural frequencies. There are both pros and cons in adopting the natural frequency change of an RC beam as a measure of its damage. The advantages are that natural frequencies are relatively easier to measure even under feeble ambient excitations, thanks to the revolutionary changes happening in the digital electronics of the measuring and data acquisition hardware. The disadvantages are that natural frequencies are relatively insensitive to the damages. However if mode shapes and static deflected

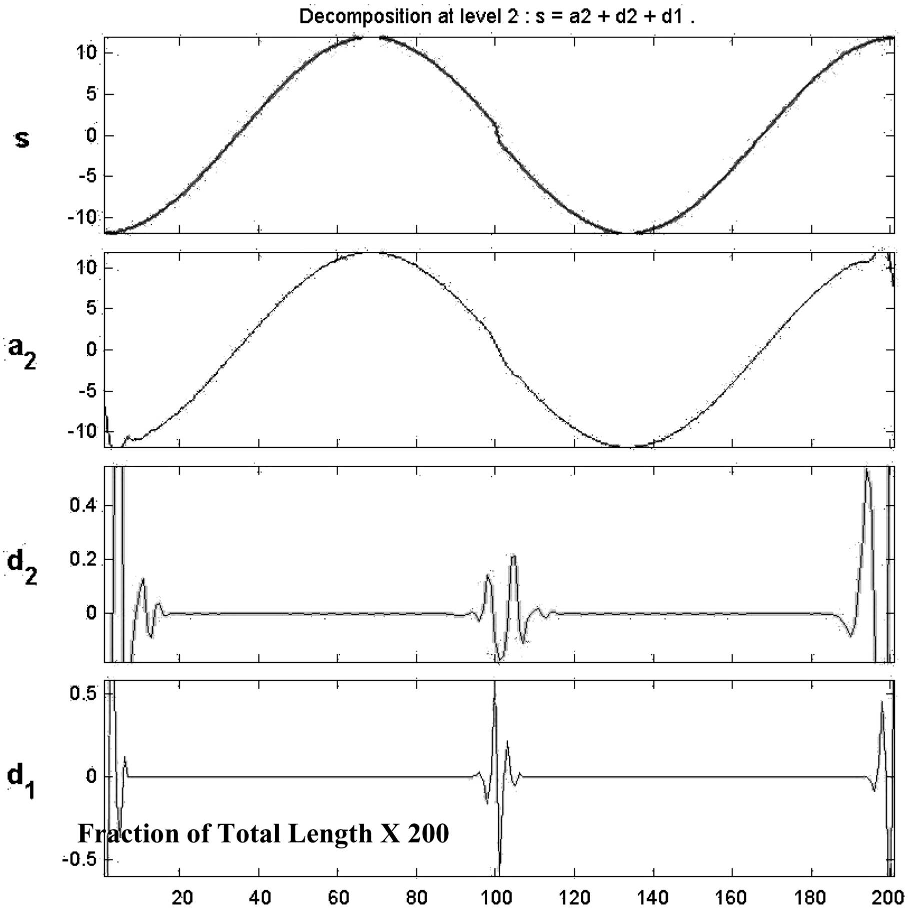

Fig. 13 Wavelet multi resolution analysis of the rotation mode shape for steel beam – Mode-III

shapes are measured and subjected to wavelet analysis, and then compared with un-damaged state, the damage shows up in the form of perturbations in the wavelet coefficients of a multi-resolution analysis. Though wavelet analysis has been already put forth into use for damage identification, the damage scenario of a reinforced concrete structural member is seldom analyzed using wavelet techniques.

A theoretical study of a wavelet analysis of the mode shapes of a flexure-dominated reinforced concrete beam subjected to progressively increasing loads is presented (Fig. 15). The span of the beam is 5 m. The depth and width of the beam are 250 and 450 mm respectively. The beam is equally reinforced both on the compression and tension faces with 400 mm^2 of steel area in the two faces. A uniformly distributed load is assumed to act on the beam. The moment curvature relationship of the beam is developed through a computer program and the tri-linear relationship between the two parameters is established (Fig. 16). The three distinct points on the M-ϕ curve are the initial cracking moment, steel-yielding moment and the moment due to the ultimate compressive strain of concrete. Slope of the tri-linearly approximated M-ϕ curve give the effective flexural rigidity (EI) of the beam span at different sections, depending on the bending moment applied at that section.

However effective EI increases mid way between cracks but decreases near crack tips due to tension

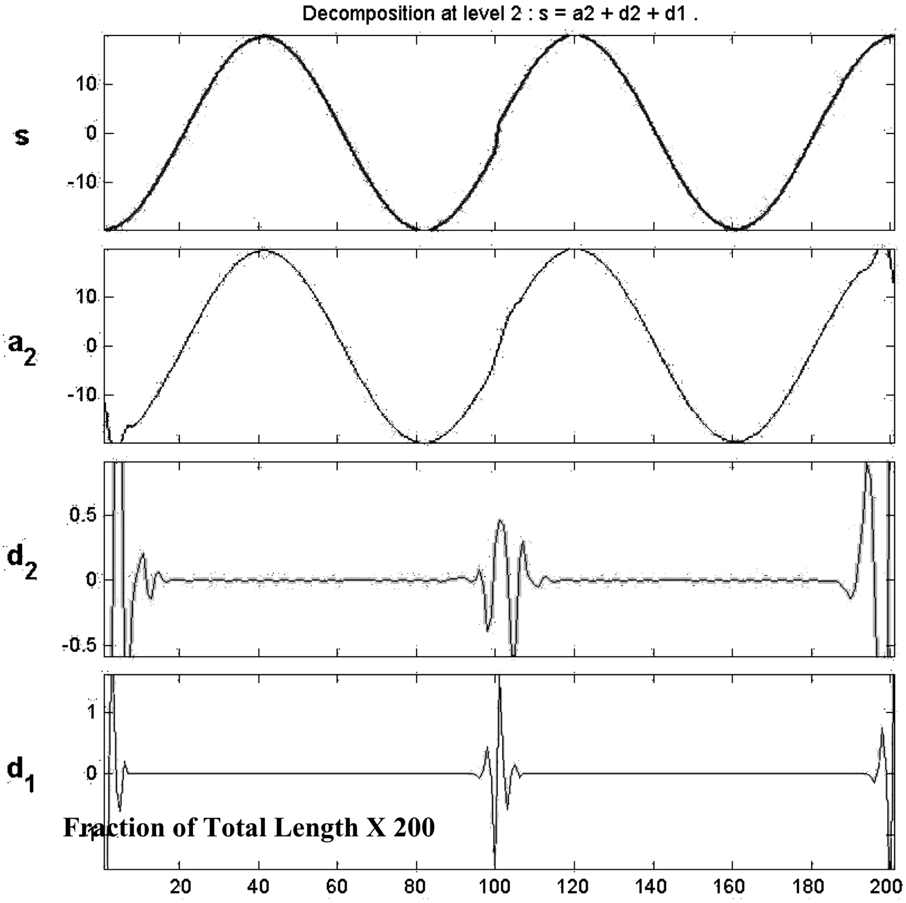

Fig. 14 Wavelet multi resolution analysis of the rotation mode shape for steel beam – Mode-V

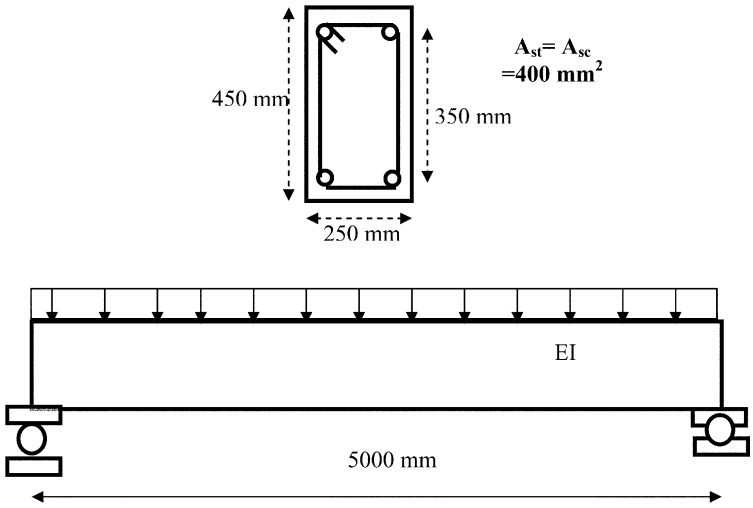

Fig. 15 RC section used in analysis with uniformly distributed load

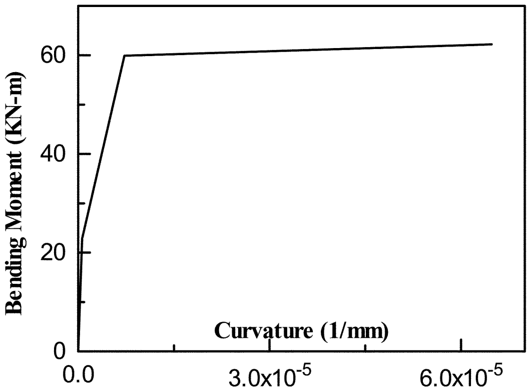

Fig. 16 Moment curvature relationship of RC section

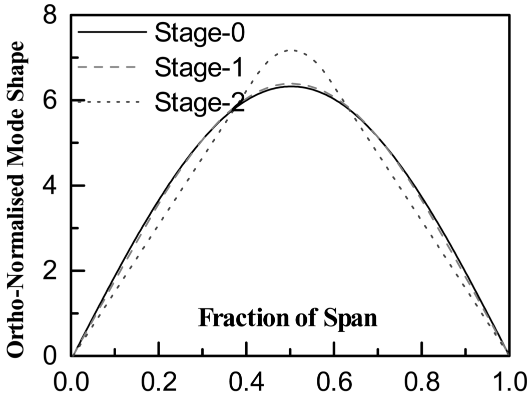

Fig. 17 Displacement mode shape of RC beam – Mode-1

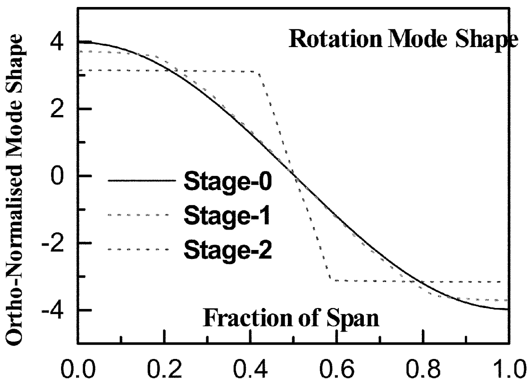

Fig. 18 Rotation mode shape of RC beam – Mode-1

stiffening of the un-cracked regions. This is approximately modeled with a sinusoidal profile of EI variation, over and above the mean EI profile, once the crack spacing and the fluctuation in EI are given as input. The computer program picks up the appropriate value of EI from the tri-linear moment

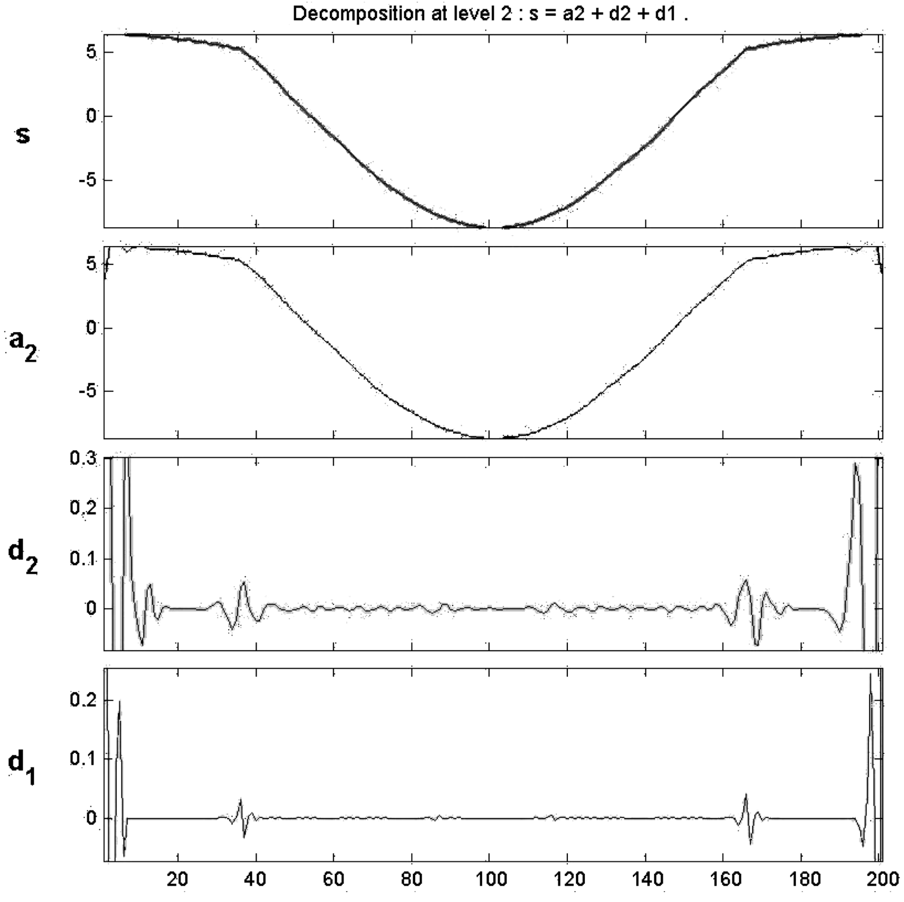

Fig. 19 Wavelet multi resolution analysis of the rotation mode shape; Mode-II, Stage-I

curvature relationship, adds up the local fluctuation in EI due to tension stiffening and uses that as the element property for stiffness assembly. The Eigenvalue run is performed through sub-space iteration and the first five modes are extracted. The dynamic free vibration analysis of the damaged beam is carried out at two stages of loading, namely, when the maximum mid-span moment on the beam is between the concrete-cracking and steel yield zones (Stage-1) and also when the moment is between steel yield and ultimate concrete compressive strains (stage-2). Stage-0 is defined as the un-damaged state prior to concrete cracking. Figs. 17 and 18 show the displacement and rotation mode shapes of the beam, for the fundamental flexural mode of the beam at all the three stages. At stage–I, a distinct discontinuity of slopes is seen near the supports, demarcating the un-cracked and cracked zones. Similarly, during stage-II, a discontinuity occurs near the mid-span demarcating the yield and cracked zones.

The wavelet analysis is then performed for these mode shapes both for displacements as well as rotations. Before the on set of cracking moment, the beam acts like a homogeneous section with no major detail coefficients. In between cracking and yield moments, there are three zones of major disturbances in a beam, characterized by initial and end zones with no cracking and the middle zone

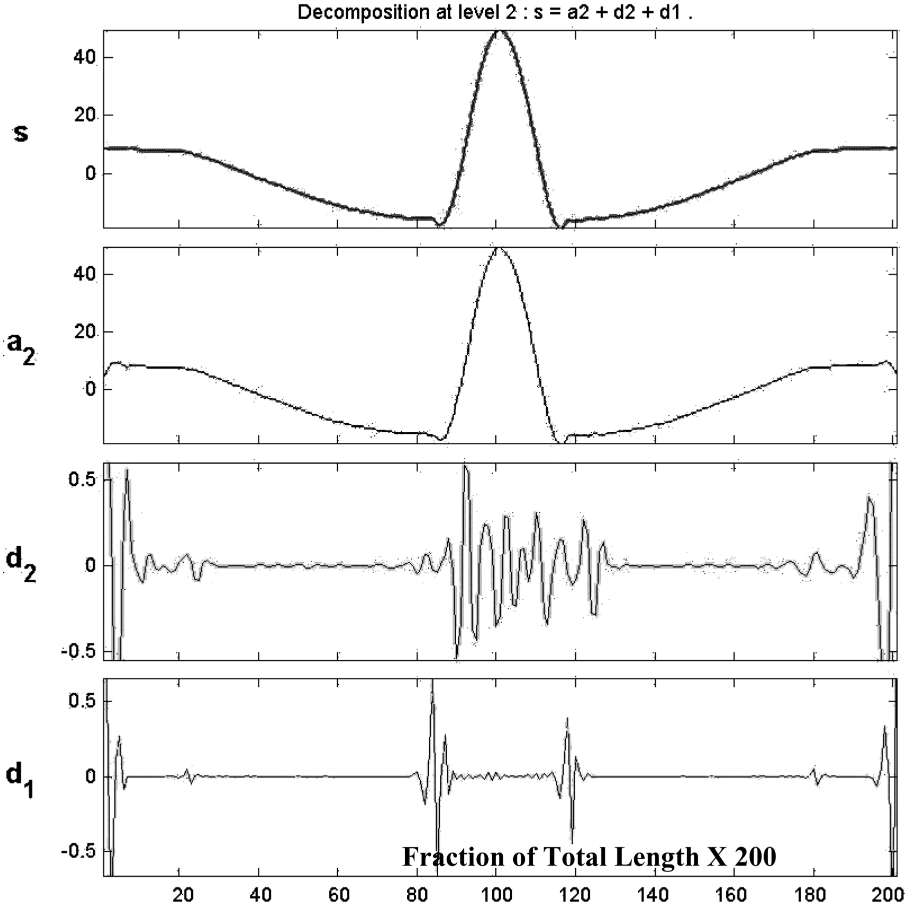

Fig. 20 Wavelet multi resolution analysis of the rotation mode shape; Mode-IV, Stage-II

with cracked concrete. Beyond yielding moment and below ultimate moment, there are five zones, characterized by initial and end zones with no cracking and the middle zone with steel yielding and the sandwiched zone with concrete cracking but without steel yielding. These different zones of abrupt changes are typically captured by wavelet analysis of the spatially varying deformation signal and are seen in Figs. 19 and 20. The transition zone between the cracked and un-cracked portions is not apparent at lower modes but multi-resolution analysis of higher modes captures all the five zones in the beam. Small ripples are also seen in these plots, which represent the local variation of EI in between two cracks.

8. Damage localization and forcing curvature nodes to desired locations

It is seen that the values of detail (D) coefficients, in a wavelet multi-resolution analysis which represent the spatial local disturbances (or higher frequency variations) are enhanced with rotation and curvature measurements and becomes further strong under higher modes. In the case of a simply supported beam representing a bridge beam, curvature and displacement nodes appear at pre-determined locations for mode shapes. If a damage occurs at a node location (zero amplitude location) corresponding to a particular mode, then measurements have to be repeated at some other mode so that the region of interest falls in the anti-node location. Towards solving this problem, a method is devised such that the point of interest shall lie in the peak region of curvature variation. The method is illustrated using two examples for a simply supported beam, but could be easily extended to any other beam with arbitrary boundary conditions. However the sacrifice to be made for picking up the peak curvature position at any arbitrary location is that the vibration shape corresponds to excitation frequency, which is off-resonance and in between two natural frequencies. This requires the excitation force to be higher, to get the same high amplitudes at resonance.

Steady state deflected shape of a beam vibrating between N and N+1$^{\text{th}}$ mode of a beam is given using the following expression, assuming that modes other than N and N+1 have reduced magnification factors and do not participate in the response. Away from resonances, the effect of damping is negligible and this effect is also not taken into account. The excitation is applied at a distance of 'c' from the left end and the response is measured at distances 'a' and 'b' from left end. ω_1 is the first flexural frequency of the system and w is the excitation frequency.

$$y(x) = \frac{1}{0.5M}\left[\frac{1}{(N^4\omega_1^2-\omega^2)}\sin\left(\frac{N\pi c}{l}\right)\sin\left(\frac{N\pi x}{l}\right)+\frac{1}{((N+1)^4\omega_1^2-\omega^2)}\sin\left(\frac{(N+1)\pi c}{l}\right)\sin\left(\frac{(N+1)\pi x}{l}\right)\right] \quad (12)$$

$$y''(x) = \frac{\pi^2}{0.5Ml^2}\left[\frac{N^2}{(N^4\omega_1^2-\omega^2)}\sin\left(\frac{N\pi c}{l}\right)\sin\left(\frac{N\pi x}{l}\right)+\frac{(N+1)^2}{((N+1)^4\omega_1^2-\omega^2)}\sin\left(\frac{(N+1)\pi c}{l}\right)\sin\left(\frac{(N+1)\pi x}{l}\right)\right] \quad (13)$$

Assuming that curvature nodes lie at 'a' and 'b' from origin, gives rise to the condition conditions that $y''(a) = y''(b) = 0$.

Simplifying Eq. (13)

$$1+\frac{\sin\left(\frac{(N+1)\pi c}{l}\right)\sin\left(\frac{(N+1)\pi a}{l}\right)(N^4\omega_1^2-\omega^2)(N+1)^2}{\sin\left(\frac{N\pi c}{l}\right)\sin\left(\frac{N\pi a}{l}\right)((N+1)^4\omega_1^2-\omega^2)N^2} = 0 \quad (14)$$

Similarly for the second condition,

$$1+\frac{\sin\left(\frac{(N+1)\pi c}{l}\right)\sin\left(\frac{(N+1)\pi b}{l}\right)(N^4\omega_1^2-\omega^2)(N+1)^2}{\sin\left(\frac{N\pi c}{l}\right)\sin\left(\frac{N\pi b}{l}\right)((N+1)^4\omega_1^2-\omega^2)N^2} = 0 \quad (15)$$

Assuming further simplification like

$$\frac{\sin\left(\frac{(N+1)\pi a}{l}\right)}{\sin\left(\frac{N\pi a}{l}\right)} = \frac{\sin\left(\frac{(N+1)\pi b}{l}\right)}{\sin\left(\frac{N\pi b}{l}\right)} = \beta \tag{16}$$

$$\frac{\sin\left(\frac{N\pi c}{l}\right)((N+1)^4\omega_1^2-\omega^2)N^2}{\sin\left(\frac{(N+1)\pi a}{l}\right)(N^4\omega_1^2-\omega^2)(N+1)^2} = -\beta \tag{17}$$

The above sets of equations suggest that once the position of 'a' is determined, 'b' is also automatically known, satisfying Eq. (16). Further, if the excitation point 'c' is known, Eq. (17) could be used to find out the excitation frequency (ω).

For evaluating the localized span, at the center of which the curvature is maximized, Eq. (16) is written as,

$$\sin\left(\frac{(N+1)\pi a}{l}\right) = -\sin\left(\frac{(N+1)\pi b}{l}\right)$$

$$\frac{(N+1)\pi a}{l} + \pi = \sin\frac{(N+1)\pi b}{l}$$

$$\sin\left(\frac{N\pi a}{l}\right) = -\sin\left(\frac{N\pi b}{l}\right)$$

$$\frac{N\pi a}{l} + \pi = \frac{N\pi b}{l} \tag{18}$$

Solving Eq. (16), in this manner is not exact, nevertheless, it throws light on the approximate value of the positions of 'a' and 'b' for particular pair of modes 'N' and 'N+1'.

Two different equations yield two different values relating 'a' and 'b'. They are,

$$\frac{(N+1)\pi a}{l} + \pi = \frac{(N+1)\pi b}{l}$$

$$(b-a) = \frac{l}{(N+1)}$$

$$\frac{N\pi a}{l} + \pi = \frac{N\pi b}{l}$$

$$(b-a) = \frac{l}{N}$$

$$(b-a)_{ave} = \frac{1}{2}\left[\frac{l}{(N+1)} + \frac{l}{N}\right] \tag{19}$$

Hence the value of pseudo span is approximated as the average of the pseudo spans corresponding

$(N + 1)$ and N^{th} modes.

After finding the value of 'a' and 'b', the excitation location 'c' is varied, such that $y''\left(\frac{a+b}{2}\right)$ is maximized.

8.1. Case study-1

It is required to create an arbitrary span, with damage location at $(a + b)/2 = 0.4$ for $N = 2$. Average span is given by Eq. (19), and predicted as 0.417. Hence 'a' and 'b' values are predicted as 0.192 l and 0.608 l (where 'l' is the span of the beam). β has to be found for these values of 'a' and 'b'. β is found as 1.03 for $a = 0.192$ and 0.86 for $b = 0.608$. After slight adjustments, 'a' and 'b' are found as 0.2 and 0.6, which yield the same value of β (=1.0).

The curve $\left(\sin\frac{(N+1)\pi a}{l}\right) / \left(\sin\frac{N\pi a}{l}\right)$ is plotted and shown in Fig. 21. The value of curvature for different locations of 'c' (excitation position) is then obtained and plotted in Fig. 22. Excitation

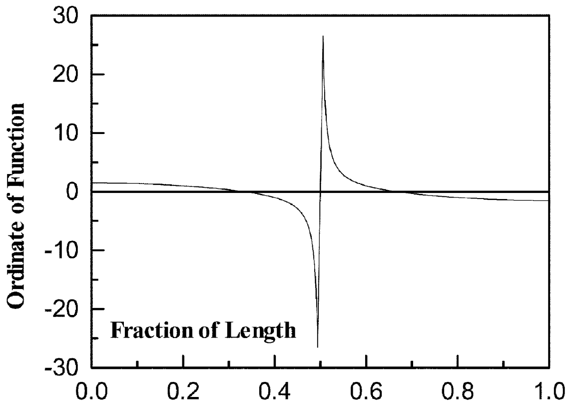

Fig. 21 Variation of β for N=2 (Case study-1)

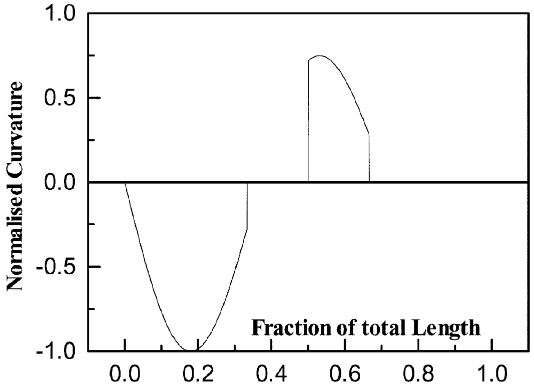

Fig. 22 Curvature distribution for different excitation positions (Case study-1)

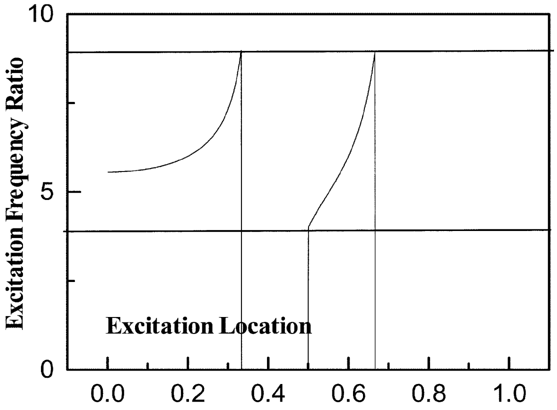

Fig. 23 Variation of excitation frequencies for different excitation locations (Case study-1)

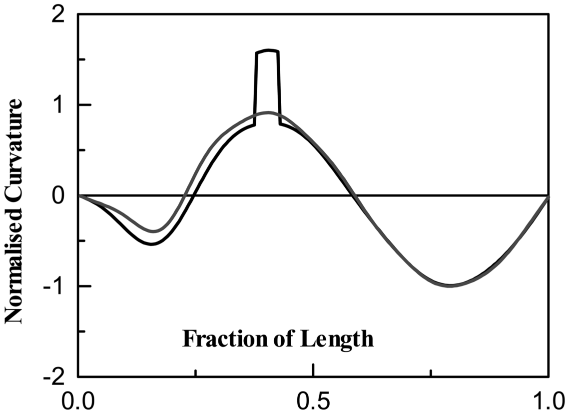

Fig. 24 Variation of curvatures for the defective and normal beams (Case study-1)

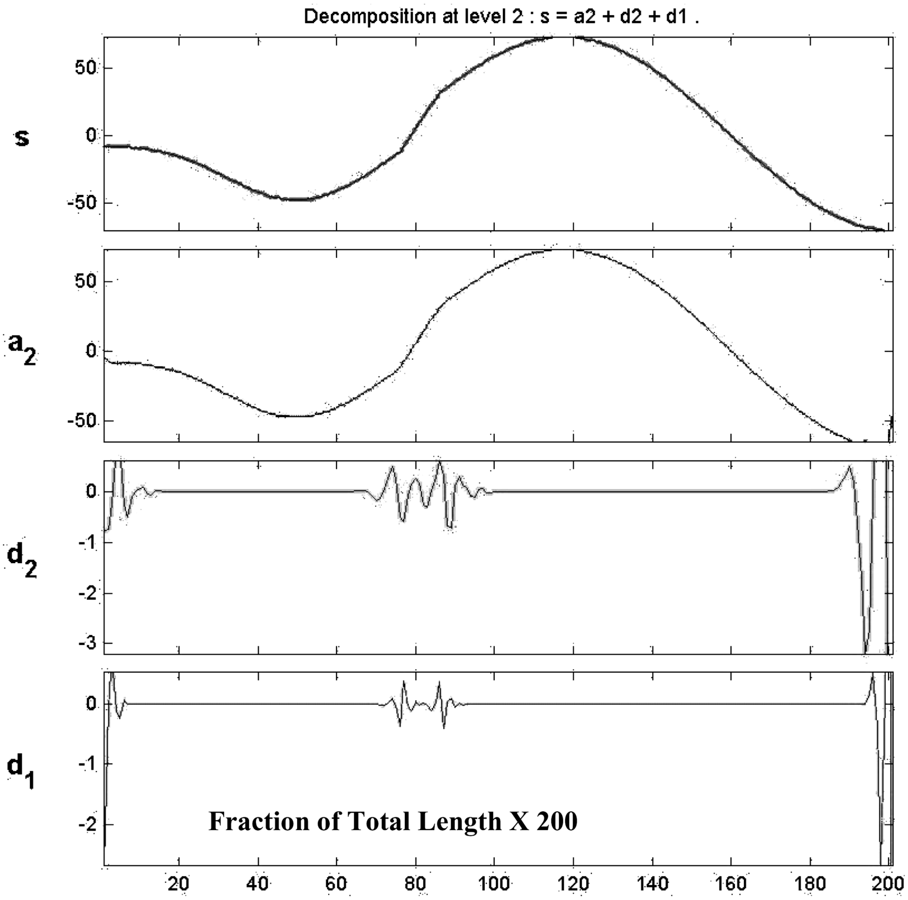

Fig. 25 Wavelet multi-resolution analysis of rotation profile (Case study-1)

frequency corresponding to different excitation locations is plotted in Fig. 23. As the position of excitation force and the frequency is known an actual steady state dynamic analysis is performed with ten flexural modes participating in the response. The curvature variation for both normal and defective beams is then plotted in Fig. 24. The defect is introduced in the form of 50% reduction in (EI) for a length of 0.25 m and situated at 0.4 l. Fig. 25 shows the wavelet multi-resolution analysis of the steady state rotation profile of the investigated beam in case study-1.

8.2. Case study-2

This is similar to case study-1, except that damage location is at 0.2 l and the pseudo span length, which has the damage location at its center has to be at 0.2 l. N is chosen as 5 and the damage location is close to the node position of both the fifth and sixth modes. Average span is calculated as 0.18 l. After a few trials and from the curve showing the b variation (Fig. 26), 'a' and 'β' values are fixed as 0.1 and 0.2755 respectively giving rise to a constant value of β (0.9511). The center of this curve is 0.19 l, which is near about the assumed damage position. Curvature variation using the N and $(N+1)^{\text{th}}$ modes is plotted in Fig. 27. The corresponding excitation frequencies are shown in Fig. 28. Using these values of

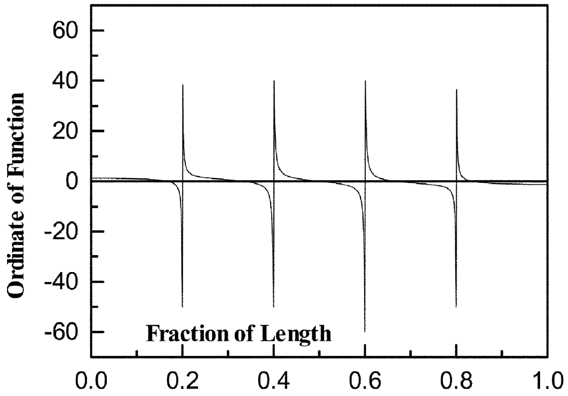

Fig. 26 Variation of β for N=5 (Case study-2)

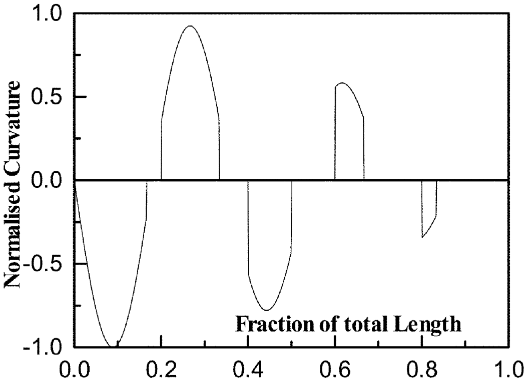

Fig. 27 Curvature distribution for different excitation positions (Case study-2)

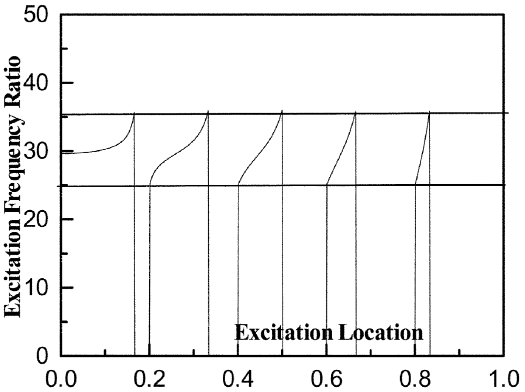

Fig. 28 Variation of excitation frequencies for different excitation locations (Case study-2)

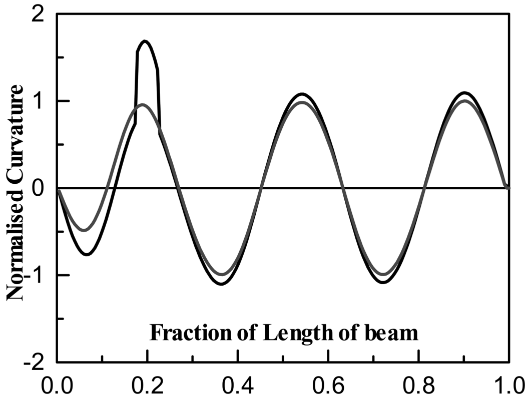

Fig. 29 Variation of curvatures for the defective and normal beams (Case study-2)

excitation location and frequency, actual dynamic analysis, using ten flexural modes is performed and the resulting curvature variations along the span is shown in Fig. 29, for both the normal and defective beams. The defect is introduced in the form of 50% reduction in (EI) for a length of 0.25 m and situated at 0.2 l. Fig. 30 shows the wavelet multi-resolution analysis of the steady state rotation profile of the investigated beam, in case study-2. The validity of the developed method is thus established.

9. Measurement of dynamic rotation using scanning laser doppler vibrometer (SLDV)

It is already stated and numerically proved that higher order modal values of rotation and curvatures are the better indicators of damage. A simplified scheme is suggested such that the dynamic rotation could be measured. One of the available measuring schemes for rotation measurement is using the scanning laser Doppler vibrometer (SLDV). SLDV can be used to perform a small amplitude linear scan at a frequency Ω, along a line between two points of interest, while the measured surface is

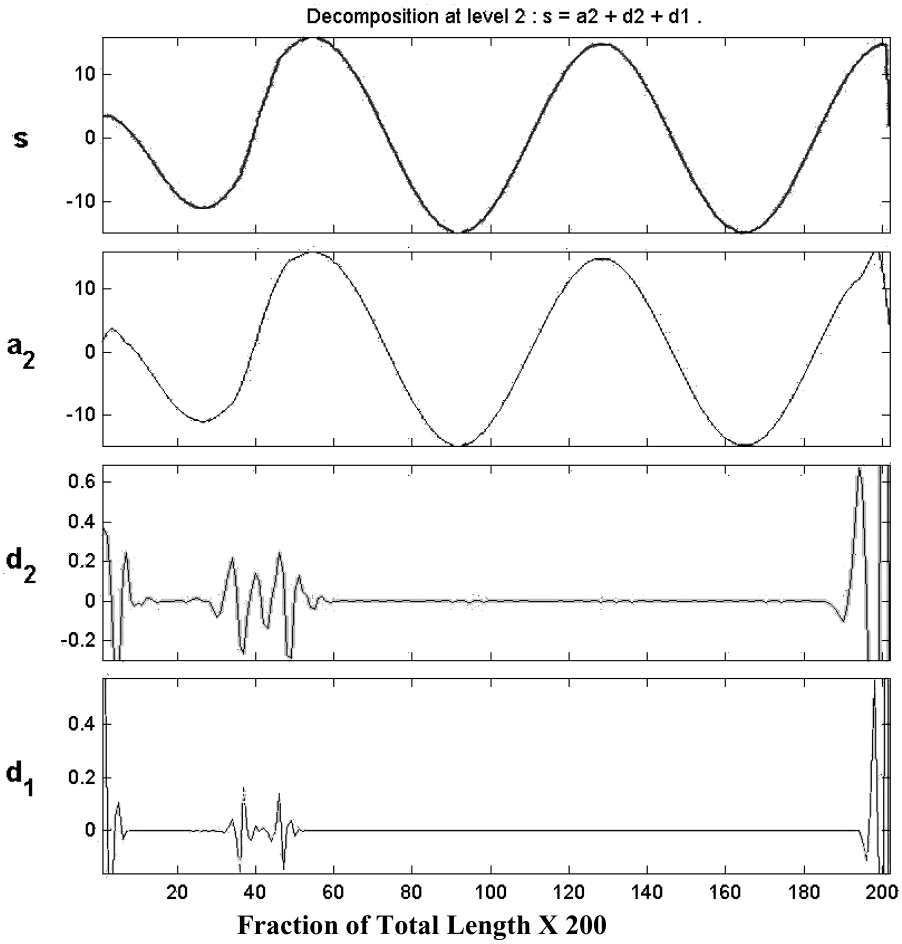

Fig. 30 Wavelet multi-resolution analysis of rotation profile (Case Study-2)

undergoing a steady state vibration with a frequency of ω. The resulting amplitude modulated signal has three frequency components in its FFT plot, with a central peak at ω and two side lobes at ω-Ω and $\omega + \Omega$. The technique can be extended to a small diameter circular scan, around a point of interest such that three dynamic response quantities, namely $z(t)$, θ_x(t) and $\theta_y(t)$ on the surface can be measured. X any Y axis are on the plane of the surface of vibration and Z is normal to the plane. The following expression can be used to deduce the above parameters using the measurement and the resulting FFT (Ewins 2000).

$$\begin{aligned}
\mathrm{Re.}(Z) &= \mathrm{Re.}(V_\omega) \\
\mathrm{Im.}(Z) &= \mathrm{Im.}(V_\omega) \\
\mathrm{Re.}(\theta_x) &= (\mathrm{Im.}(V_{\omega+\Omega}) - \mathrm{Im.}(V_{\omega-\Omega}))/r \\
\mathrm{Im.}(\theta_x) &= (\mathrm{Re.}(V_{\omega-\Omega}) - \mathrm{Re.}(V_{\omega+\Omega}))/r \\
\mathrm{Re.}(\theta_y) &= (\mathrm{Re.}(V_{\omega+\Omega}) + \mathrm{Re.}(V_{\omega-\Omega}))/r \\
\mathrm{Im.}(\theta_y) &= (\mathrm{Im.}(V_{\omega-\Omega}) - \mathrm{Im.}(V_{\omega+\Omega}))/r
\end{aligned} \tag{20}$$

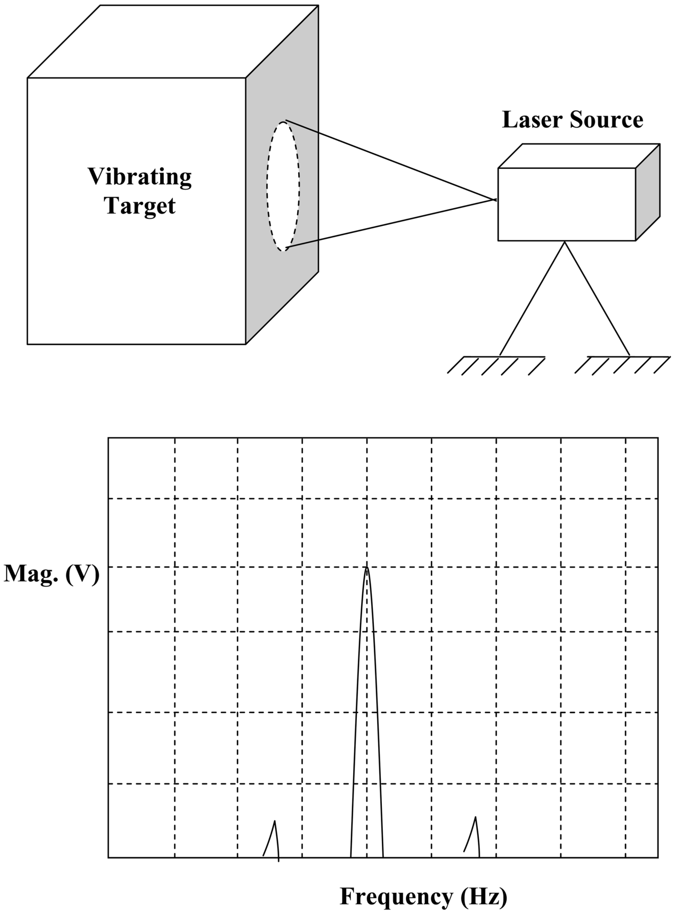

Fig. 31 A scheme for measuring rotation using a scanning laser vibrometer and the FFT of the scanned data

where r is the radius of scan and Re. and Im. are the real and imaginary values of measurement. Fig. 31 shows the typical measuring scheme and the corresponding FFT performed on the measurement. Dynamic curvature could be obtained as the first derivative of rotation.

10. Conclusions

Free vibration mode shape and the static deflected shape of a damaged structural beam element is computed and subjected to multi-resolution wavelet analysis. The damage modeling is done by two methods, one representing a rotational spring to model the crack location (Model-1) and the other one with changing $(EI)_{eff}$ values depending on the bending moment at that section (Model-2). Model-1 is typically used for idealizing cracked locations in steel beams and the appropriate spring stiffnesses are derived using fracture mechanics principles. Model-2 is suitable for stiffness, deflection and mode shape computation of reinforced concrete flexure-dominating elements. $(EI)_{eff}$ values are obtained through M-ϕ relationship of the section. The dynamic free vibration response is computed at two damaged states of the reinforced concrete beam element, one between cracking and yield moments and the other one between the yield and ultimate moments.

Daubechies (DB4) and bi-orthogonal (BIOR 6.8) family of scaling and wavelet functions are used for the computation of the approximate (A) and detail (D) functions. Two level multi-resolution analysis is found to be sufficient to capture the disturbances in the deformation profile. Displacement, rotation and curvatures are used as damage indicators and their relative performance suggests that rotation and curvatures are better damage indicators as compared to displacements. Rotation mode shapes are not that difficult to measure and laser based non-contact vibration meters employing Doppler effects are already in vogue, which can scan a small area and report the local dynamic rotations. Higher order modes, are particularly suitable and those modes where the curvature shows peaks are the ideal ones for damage detection. It may be surmised that static deflected shapes and lower mode displacement profiles may show disturbances in the wavelet detail coefficients but possibly may get submerged in the instrument noise of the measuring system.

A method is devised such that curvature nodes could be forced at arbitrary points of interests and the mid locations of these pseudo spans can be observed for potential cracks. This method could be adopted if a curvature peak is automatically not coming in an anti-node location of a resonating beam. The method is illustrated for a simply supported beam and could be extended to any arbitrary linear structural member provided mode shape and frequency information is available for higher modes.

Acknowledgements

The paper is published with the approval of Director, Structural Engineering Research Centre, Chennai, India.

References

Abdo, M. A. B. and Hori, H. (2002), “A numerical study of structural damage detection using changes in the rotation of mode shapes”, *J. Sound. Vib.*, **251**(2).

Abdel Wahab, M. M. and Roeck, G. D. (1999), “Damage detection in bridges using modal curvatures: Application to a real damage scenario”, *J. Sound. Vib.*, **226**(2), 217-235

Daubechies, I. (1992), *Ten Lectures on Wavelets*, SIAM, Philadelphia.

Ewins, D. J. (2000) *Modal Testing: Theory Practice and Applications,* Research Studies Press Ltd, Hertfordshire.

Gurley, K. and Kareem, A. (1999), “Applications of wavelet transforms in earthquake wind and ocean engineering”, *Eng. Struct.*, **21**, 149-167.

Hassiotis, S. (2000), “Identification of damage using natural frequencies and Markov parameters”, *Comput. Struct.*, **74**, 365-373.

Hassiotis, S. and Jeong, G. D. (1993), “Assessment of structural damage from natural frequency measurements”, *Comput. Struct.*, **49**(4), 679-691.

Hera, A. and Hou, Z. (2004), “Application of wavelet approach for ASCE structural health monitoring benchmark studies”, *J. Eng. Mech.*, 96-104.

Hou, Z, Noori, M. and Amand, R. S. (2000), “Wavelet based approach for structural damage detection”, *J. Eng. Mech.*, 677-683.

Hubbard, B. B. (2003), *The World According to Wavelets*, Universities Press (India), Second Edition.

Kim, H. and Melhem, H. (2004), “Damage detection of structures by wavelet analysis”, *Eng. Struct.*, **26**, 347-362.

Lakshmanan, N., Srinivasulu, P. and Parameswaran, V.S. (1991), “Post cracking stiffness and damping in reinforced concrete beam elements”, *J. Struct. Eng.*, **17**(4), 1405-1411.

Liew, K. M. and Wang, Q. (1998), "Application of wavelet theory for crack identification of structures", *J. Eng. Mech.*, 152-157.
Mallat, S. A. (1998), *Wavelet Tour of Signal Processing,* Academic Press, Boston.
Melhem, H. and Kim, H. (2003), "Damage detection in concrete by fourier and wavelet analysis", *J. Eng. Mech.*, 571-577.
Ovanesova, A. V. and Suarez, L. E. (2004), "Application of wavelet transforms to damage detection in frame structures", *Eng. Struct.*, **26**, 39-49.
Owolabi, G. M., Swamidas, A. S. J. and Seshadri, R. (2003), "Crack detection in beams using changes in frequencies and amplitudes of frequency response functions", *J. Sound. Vib.*, **265**, 1-22.
Pandey, A. K., Biswas, M. and Samman, M. M. (1991), "Damage detection from changes in curvature mode shapes", *J. Sound Vib.*, **145**, 312-332.
Raghuveer, M. R. and Boppardikar, A. S. (2001), *Wavelet Transforms – Introduction to theory and applications*, Pearson education Asia.
Rajagopalan, N., Lakshmanan, N. and Jeyasehar C. A. (1999), "Damage assessment in reinforced concrete beams using natural frequencies", *J. Struct. Eng.*, India, **26**(3), 165-172.
Rajagopalan, N., Lakshmanan, N. and Muthumani, K. (1996), "Stiffness degradation of reinforced concrete beams under repeated low energy impact loading", *Indian Concrete J.*, **69**(4), 227-234.
Ratcliffe, C P. (2000), "A frequency and curvature based experimental method for locating damage in structures", *Transactions of ASME*, **122**, 324-329
Sheinman, I. (1996), "Damage detection and updating of stiffness and mass matrices using mode data", *Comput. Struct.*, **59**(1), 149-156

Notation

EI	: Flexural Rigidity of the Beam Section
α	: Ratio of Change in Flexural Rigidity
f_{ck}	: Characteristic Strength of Concrete
ψ	: Wavelet Mother Function
ϕ	: Wavelet Scaling Function
$C(a, b)$	: Wavelet Coefficients corresponding to translation (a) and dilation (b) values
$A(x)$ and $D(x)$	: Approximate and Detail Functions
N, N+1	: Integers corresponding to N and $N+1$ modes
ω_1	: first flexural frequency of the system
ω	: the excitation frequency.
a, b	: Start and end position of pseudo span, reckoned from left end of the beam
c	: Load application point from left end of the beam
β	: Function defined as $\dfrac{\sin\frac{(N+1)\pi a}{l}}{\sin\frac{N\pi a}{l}}$
CC	